Article

Photodegradation of 1,2,4-Trichlorobenzene on Montmorillonite–TiO$_2$ Nanocomposites

Beatriz González [1], Bárbara Muñoz [1], Miguel Angel Vicente [1,*] , Raquel Trujillano [1], Vicente Rives [1] , Antonio Gil [2] and Sophia Korili [2]

[1] GIR-QUESCAT-Departamento de Química Inorgánica, Universidad de Salamanca, 37008 Salamanca, Spain; bei@usal.es (B.G.); barbaramm@usal.es (B.M.); rakel@usal.es (R.T.); vrives@usal.es (V.R.)

[2] INAMAT-Departamento de Ciencias, Universidad Pública de Navarra, 31006 Pamplona, Spain; andoni@unavarra.es (A.G.); sofia.korili@unavarra.es (S.K.)

* Correspondence: mavicente@usal.es; Tel.: +34-670-55-83-92

Abstract: Montmorillonite–TiO$_2$ nanocomposites were prepared using two different methods (ultrasonic or stirring) and using titanium(IV) isopropoxide as precursor. The solids were characterized by element chemical analysis, X-ray diffraction, FTIR spectroscopy, thermal analyses, and nitrogen adsorption. The evolution of the properties as a function of the preparation method was discussed. These nanocomposites were used as catalysts for the photodegradation of 1,2,4-trichlorobenzene. The degradation pathway and the nature of the by–products were investigated by mass spectrometry.

Keywords: nanocomposites; montmorillonite; TiO$_2$; 1,2,4-trichlorobenzene; photocatalytic degradation

1. Introduction

Clay minerals are very abundant natural minerals, with particular properties and a large number of important applications. They result from rock weathering, alternating hydrothermal and sedimentary deposits. The clay mineral used in the present work is montmorillonite, which is the most representative clay mineral of the smectite group. Clay minerals have been widely used for the development of catalysts. Clay minerals are catalysts themselves, and their surface properties can be tailored upon submission to different physicochemical treatments (acid activation, thermal activation, pillaring ...). They are excellent supports for other active phases. Clay minerals are currently recognized as efficient catalysts in reactions that involve fine chemistry, redox transformations, organic synthesis, acid catalysis, among others [1,2].

Pillaring is a molecular engineering-based method consisting in treatment of clays, mainly smectites, with metallic polyoxocations. The resulting materials are named Pillared Interlayered Clays (PILCs) and, among them, Ti-PILCs have been very studied [3,4]. Due to its photoelectric properties, low cost, resistance to corrosion, non–toxicity and chemical stability in a wide pH range [5], TiO$_2$ is a functional, versatile material and effective photocatalyst in environmental decontamination. TiO$_2$ has three polymorphic structures, namely, anatase, rutile and brookite. Anatase has the highest catalytic activity, while rutile is inactive in the photodegradation of organic compounds, probably due to its low capacity for O$_2$ adsorption [6].

The difficulty to tailor the size of the pillars or the pore structure limits the applications of PILCs. However, the synthesis of nanostructures composed of TiO$_2$ and swellable clay minerals has been recently reported, the nanostructures exhibiting photocatalytic properties even higher than those of commercial Degussa P25 TiO$_2$ [6]. As the heterogeneous photocatalytic reactions occur on the surface of the catalysts, adsorption of the substrate molecules onto the TiO$_2$ particles is a critical point for their degradation [7–11]. Therefore, in order to increase the number of active surface sites to generate

OH● radicals and to improve the interaction with pollutants [10,11], in most of the studies dealing with photocatalysts based on TiO$_2$ particles, these are dispersed on the surface of silica, alumina, clays or zeolites. Clays are receiving in recent years a large attention as supports for these photocatalysts, since they are able to adsorb organic substances on their external surfaces, as well as within their interlayer spaces, favoring the contact with the photoactive phase [12–22]. In this context, the use of ultrasounds for incorporation of TiO$_2$ on clays, scarcely explored in the past [23], appears as an interesting alternative.

1,2,4-trichlorobenzene (TCB) is an organochlorine compound derived from benzene with three chlorine substituents. It is a colorless solvent with a characteristic aromatic odor, insoluble in water and slightly soluble in ethanol. TCB is used as a solvent in the chemical industry, for pigments, dielectric fluid, synthetic oil for transformers, heat transfer media and in lubricants and insecticides. Exposure to TCB may cause changes in liver, kidneys and adrenal glands; the Maximum Contaminant Level Goal (MCLG) fixed by EPA for this contaminant is 0.07 ppm.

The aim of the present work is to prepare montmorillonite–TiO$_2$ nanocomposites, by simple preparation methods, namely, the ultrasonic method or traditional agitation. The structural and textural characteristics of the solids obtained by both methods are compared, and preliminary studies on their catalytic performance in the photodegradation of 1,2,4-trichlorobenzene are reported.

2. Materials and Methods

2.1. Preparation of the Catalysts

The clay mineral used was a natural montmorillonite from Cheto, AZ, USA, denoted as SAz–1 in The Clay Minerals Repository. The natural clay was purified before its use, separating the fraction lower than 2 μm [24], which was designated as 'M'. This solid was calcined at 500 °C for 2 h to be used in the photocatalytic reaction, as a reference for comparison with the nanocomposites.

Two nanocomposite samples were synthesized, varying the method of preparation using ultrasounds (bath Fungilab, Barcelona, Spain, 40 kHz, 250 W) or magnetic stirring (samples 'MTi1' and 'MTi2', respectively). An amount of 2 mL of titanium(IV) isopropoxide (Sigma-Aldrich, Madrid, Spain), 97% was added to a dispersion of 2 g of clay in 200 mL of water. In the conventional method, the dispersion was magnetically stirred overnight at room temperature; in the ultrasonic method the dispersion was stirred for 12 h and submitted to six periods of 15 min each under ultrasonic treatment. In both cases, the solids were separated by centrifugation, washed with distilled water, dried at 70 °C and finally calcined at 500 °C for 2 h.

2.2. Characterization Techniques

Element chemical analyses were carried out at Servicio General de Análisis Químico Aplicado (Universidad de Salamanca, Salamanca, Spain), using Inductively Coupled Plasma–Atomic Emission Spectrometry (ICP–AES). The powder X-ray diffraction (PXRD) patterns were recorded between 2 and 65° (2θ) over non–oriented powder samples, at a scanning speed of 2°/min, in a Siemens D–5000 diffractometer (Siemens España, Madrid, Spain), operating at 40 kV and 30 mA, and using filtered Cu Kα radiation (λ = 1.5418 Å). Raman scattering measurements were carried out at room temperature with a micro-Raman spectrometer LabRAM HR Evolution Horiba Jobin-Yvon (Horiba Abx Ibérica, Madrid, Spain), equipped with a solid-state laser operating at 532 nm and a 50× objective. The acquisition time was 2 s at each point, with a spectral resolution of 2 cm^{-1}, ten spectra were averaged, and the laser excitation power was kept below 1 mW to avoid laser-induced heating. Raman scattered light was analyzed by using a diffraction grating (600 gr mm^{-1}) and a CCD Camera. The FT–IR spectra were recorded in the 4000–450 cm^{-1} range in a PerkinElmer Spectrum–One spectrometer (Waltham, MA, USA) by the KBr pellet method (sample:KBr mass ratio 1:300). The thermal analyses were performed on a SDT Q600 apparatus (TA Instruments, Madrid, Spain), under a flow of 20 mL/min of oxygen (L'Air Liquide, Madrid, Spain, 99.999%) and a temperature heating rate of 10 °C/min from room

temperature to 900 °C. Textural properties were determined from nitrogen (L'Air Liquide, Spain, 99.999%) adsorption–desorption data, obtained at −196 °C using a Micrometrics Gemini VII 2390 t, Surface Area and Porosity apparatus (Norcross, GA, USA), after outgassing the solids for 2 h at 110 °C. The specific surface area (SSA) was obtained by the BET method, external surface area and micropore volume by means of the t-method, and the total pore volume from the nitrogen adsorbed at a relative pressure of 0.95 [25]. Scanning electron microscopy (SEM) was performed at the Pulsed Laser Center (CLPU, Salamanca, Spain) using a Carl Zeiss SEM EVO HD25 microscope (Zeiss, Carl Zeiss Iberia—Division Microscopy, Madrid, Spain); the samples had been coated with a thin gold layer by evaporation.

2.3. Reactivity Studies

For the photodegradation reaction, an MPDS–Basic system from Peschl Ultraviolet, with a PhotoLAB Batch–L reactor and a TQ150–Z0 lamp (power 150 W), integrated in a photon CABINET was used. The spectrum is continuous, with the main peaks at 366 nm (radiation flux, φ 6.4 W) and 313 nm (φ 4.3 W). In each reaction, 750 mg of clay was added to a TCB solution of 25 mg·L^{-1} in EtOH/H$_2$O (1:1 v/v). The concentration of TCB was determined by UV–visible spectroscopy, using a Thermo Electron Helios Gamma spectrophotometer (UV Consulting Peschl España, Castellón, Spain). To identify the by–products generated during UV degradation, the solutions were analyzed after various treatment times by mass spectrometry. The equipment used for this purpose was an Agilent 1100 HPLC coupled to an ultraviolet detector and an Agilent Trap XCT mass spectrometer (Agilent Technologies Spain, Las Rozas, Madrid, Spain). These analyses were carried out at Servicio Central de Análisis Elemental, Cromatografía y Masas (Universidad de Salamanca).

3. Results and Discussion

The characterization of raw montmorillonite has been reported by González-Rodríguez et al. elsewhere [24]. Its cation exchange capacity was 0.67 meq/g, its basal spacing was 13.60 Å, and its BET specific surface area was 49 m^2/g.

The element chemical analysis results of the starting montmorillonite and of the nanocomposites were included in Table 1. Due to the different degree of hydration of each solid, the sum of the oxides contents was different in each case. So, to compare the solids among them, a double normalization was carried out: first, the composition of M was calculated assuming the sum of the oxides to be 100% ("water–free composition"); secondly, SiO$_2$ was used as a sort of "internal standard", since the Si(IV) cations located in the tetrahedral layer did not suffer alteration during the treatment. The composition of the solids referred to the amount of SiO$_2$ in the starting clay is shown in Table 2.

Table 1. Chemical composition of the starting natural clay and of the synthesized solids, expressed as a percentage of oxides for each element (wt %).

Sample	SiO2	Al2O3	Fe2O3	MnO	MgO	CaO	Na2O	K2O	TiO2	Total
M	55.80	15.92	1.41	0.04	5.58	1.69	0.06	0.06	0.21	80.77
MTi1	42.65	11.48	0.98	0.04	4.08	1.18	0.17	0.07	22.71	83.36
MTi2	49.51	13.57	1.17	0.04	4.80	1.40	0.11	0.08	14.16	84.84

Table 2. Chemical composition of the samples, normalized to water–free composition and to the SiO$_2$ content in the starting montmorillonite (wt %).

Sample	SiO$_2$	Al$_2$O$_3$	Fe$_2$O$_3$	MnO	MgO	CaO	Na$_2$O	K$_2$O	TiO$_2$
M	69.09	19.71	1.75	0.05	6.91	2.09	0.07	0.07	0.26
MTi1	69.09	18.60	1.59	0.06	6.61	1.91	0.28	0.11	36.79
MTi2	69.09	18.94	1.63	0.06	6.70	1.95	0.15	0.11	19.76

As expected, there was a noticeable increase in the TiO$_2$ content in the treated solids, from 0.26% in raw montmorillonite up to 19.76% in sample MTi1 and 36.79% in sample MTi2. A slight (ca. 10% for the normalized values) decrease in the CaO content was also observed, indicating that the Ca^{2+} cations have been partially exchanged for Ti species. However, almost full exchange of Ca^{2+} cations during pillaring of this clay has been previously reported [24]. This suggested that TiO$_2$ deposition was very fast, that is, precipitation occurred before that the Ti species could polymerize and be incorporated into the solid by ion exchange. This result was not surprising, due to the strong acidity of this cation and the strict conditions necessary for its polymerization, conditions that have not been maintained in the present procedure. The contents of MgO and Fe$_2$O$_3$ slightly decreased; these cations are located in the octahedral layer and can dissolve during the treatments under the acidic conditions given by the Ti solution [26].

Obviously, the increase in the TiO$_2$ content gave rise to a relative decrease in the amount of the other oxides, but after the normalization to the internal amount of SiO$_2$ such percentages remained practically constant.

The diffractograms of the starting clay and of the prepared nanocomposites, dried at 70 °C and calcined at 500 °C, are shown in Figure 1 and the basal spacing values are summarized in Table 3. The basal spacing of the natural clay was 13.60 Å, indicating a high hydration degree. The spacing for the (06,33) reflection was 1.50 Å, which corresponded to a dioctahedral smectite, as it is the case of the used montmorillonite. Upon calcination, the layered structure was maintained, but the spacing of the 001 peak decreased to 9.57 Å, with a noticeable decrease of intensity, as a consequence of water removal and a lower ordering in the *c*-axis stacking [24].
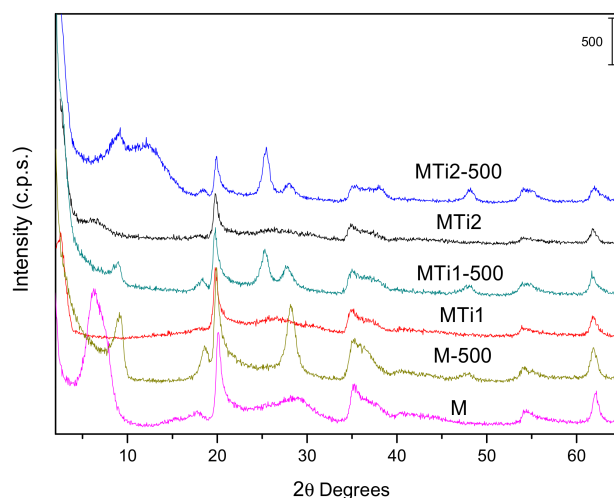

Figure 1. Powder X-ray diffractograms of the parent montmorillonite and the catalysts synthesized. For comparison, the diffractograms of dried and calcined (denoted "−500") solids are given.

Incorporation of Ti gave rise to an increase in the basal spacing of sample MTi1 (prepared by the ultrasonic method), to 34.37 Å, suggesting that large Ti-containing species have entered into the interlayer space. This did not occur by the conventional method (sample MTi2), suggesting that precipitation may be very fast under such conditions. Upon calcination, the basal spacing decreased to ca. 9.7–9.9 Å for both samples, with a parallel decrease of intensity, in agreement with the partial collapse of the layered structure. In the solid prepared by the conventional method (MTi2) a broad band appeared at ca. 8–18°, suggesting the presence of an amorphous TiO$_2$ phase, while no peak from any crystalline polymorph of this compound was observed, probably because the calcination temperature was not enough for their crystallization [27,28]. The peaks corresponding to in-plane montmorillonite diffractions (that is, not involved in the *c*-stacking of the individual layers) remained in the same positions and with similar intensities as in the parent solid, indicating that the treatments did not alter the structure of the individual layers.

Table 3. Basal spacing (Å) for the dried and calcined samples.

Sample	Dried	Calcined
M	13.60	9.57
MTi1	34.37	9.87
MTi2	14.01	9.66

As X-ray diffraction did not provide conclusive information on the nature of titanium species existing in the solids, these were studied by Raman spectroscopy. The spectra (Figure 2) showed that sample MTi1 was composed of both anatase and rutile phases, while sample MTi2 contained only anatase [29,30]. Considering that both samples were calcined under identical conditions, these results suggested that the crystallization of TiO_2 phases depended on the way the titanium precursor was reacted with montmorillonite.
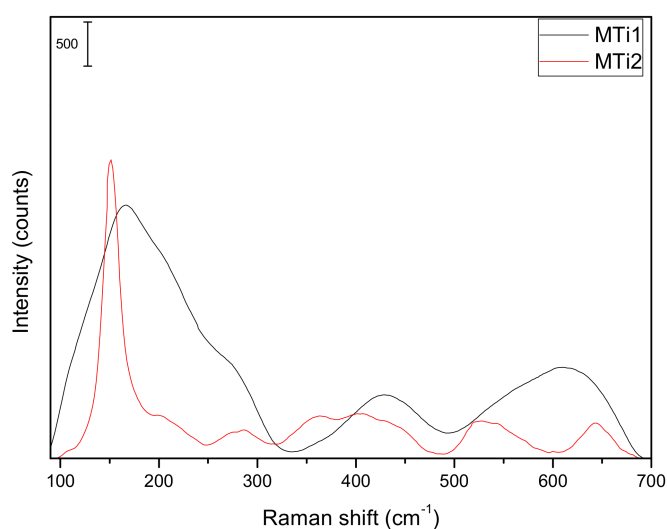
Figure 2. Raman spectra of samples MTi1 and MTi2.

Figure 3 shows the FT-IR spectra of the raw clay and of the catalysts, dried at 70 °C after preparation (that is, before calcination). Similar bands were observed for all three solids, showing that the structure of the montmorillonite was not significantly altered, and that the incorporation of Ti did not produce new bands. However, some small differences were observed; the band around 1000 cm^{-1}, characteristic of the Si–O–M–O–Si bonds in the silicate layer (M = octahedral cation), broadened and showed a shoulder at high wavenumbers for both solids after the treatments. This is in agreement with the slight decrease of Mg and Fe content upon treatment, which made that a small fraction of the clay evolved to silica [26]. On the other hand, the intensities of the M–O bands (in the low wavenumber region, 620, 518 cm^{-1}) increased, probably due to the contribution of the Ti–O vibrations after Ti incorporation. This increase was especially significant for sample MTi2, with a very high Ti content. The O–H vibration at 3609 cm^{-1} disappeared in sample MTi1 and remained in MTi2, suggesting that Ti–species effectively reacted with these OH groups in MTi1 but rapidly precipitated in MTi2, without interacting with these groups, as already suggested by other techniques. In addition, small effects due to C–H bonds were observed around 3000 cm^{-1}, assignable to contamination from organic vapors in the laboratory. These effects were more intense in MTi1, suggesting the probable presence of residual isopropoxide groups in the Ti species, as reported previously [31].
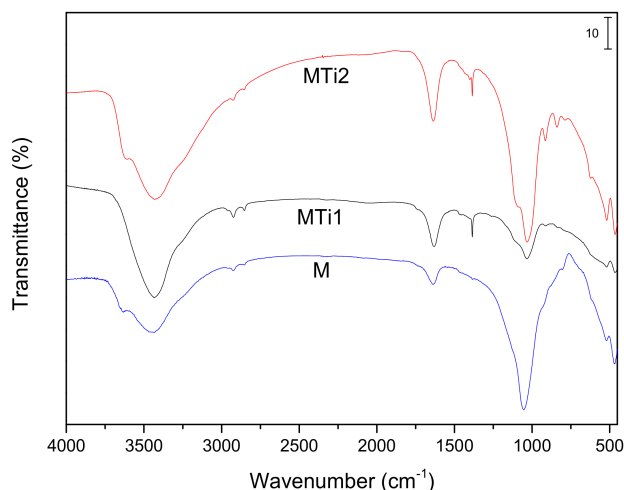
Figure 3. FT–IR spectra for the dried solids.

The thermogravimetric curve of samples MTi1 and MTi2 (Figure 4) showed a similar behavior to that of natural montmorillonite (Figure S1, Supplementary Material). A first mass loss of ~12% was recorded at low temperature, associated to an endothermic effect centered at ~100 °C, with a shoulder at 185 °C. This effect is due to the removal of surface-adsorbed water and that in the interlayer space, and also on the Ti-containing species crystallites. The shoulder suggested that a fraction of the molecules was more strongly retained, and its removal was more difficult, probably corresponding to the molecules in the interlayer space. In the central temperature range (200–600 °C), a gentle mass loss was observed, ~6%, due to the loss of the remaining water molecules bound to the surface and to dehydroxylation of the clay and of the Ti species. A slight exothermic effect was recorded around 450 °C, which may correspond to the combustion of some isopropoxide groups fixed during the preparation or, less probably, to a phase change in the Ti–containing species. The incorporation of TiO_2 did not produce other appreciable thermal effects, and the overall mass loss up to 900 °C was 18%. At 500 °C, adsorbed water and isopropoxide have been removed, but dehydroxylation has not been completed, being a suitable temperature for the calcination of the solids for the photocatalytic study.
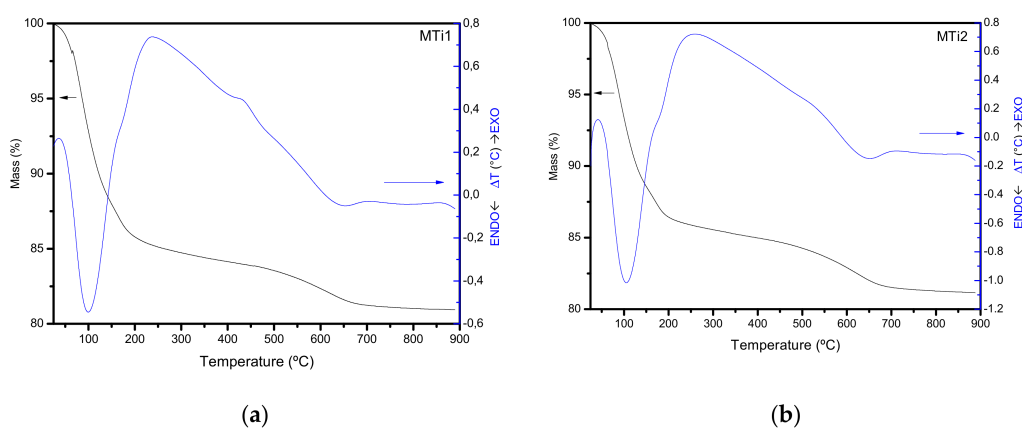

Figure 4. Thermal curves, in oxygen atmosphere, for (**a**) MTi1 and (**b**) MTi2 samples.

The textural properties of the solids were studied by N_2 adsorption–desorption at −196 °C. The isotherms for the calcined solids (Figure 5) belong to type II according to the IUPAC classification, with H4 hysteresis cycles, characteristic of solids with narrow slit pores, with a point of inflexion at a relative pressure of 0.4 [32].
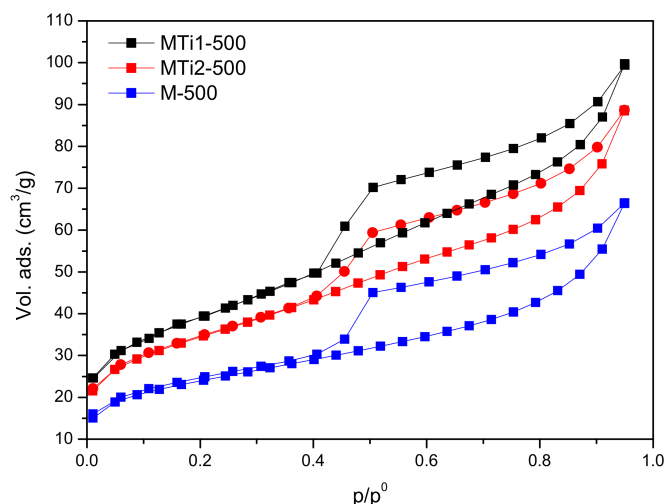
Figure 5. Nitrogen adsorption–desorption isotherms of the calcined solids.

The BET-specific surface areas, external surface areas, and micropore volumes of the solids are summarized in Table 4. The specific surface area increased for the treated solids, reaching values of 233 and 193 m^2/g for dried MTi1 and MTi2, respectively, in agreement to the incorporation of Ti species. It should be recalled that before recording the isotherms the solids were outgassed at a temperature higher than that of drying, so the specific surface areas of the dried solids actually correspond to the solids treated at the outgassing temperature. After calcination, the specific surface area increased in the natural montmorillonite from 49 to 80 m^2/g, due to the "thermal activation" caused by the calcination, with removal of water. For the treated solids, the specific surface area decreased under calcination, as expected for the transformation of the initially existing Ti-containing species to phases close to TiO_2. In all cases, most of the total BET surface area corresponded to external surface area, and consequently the micropore volume was small.

Table 4. Specific surface area (S_{BET}), external surface area (S_{ext}) and micropore volume (V_m) of natural montmorillonite [24] and of the catalysts.

Sample	Dried			Calcined		
	S_{BET} (m^2/g)	S_{ext} (m^2/g)	V_m (cm^3/g)	S_{BET} (m^2/g)	S_{ext} (m^2/g)	V_m (cm^3/g)
M	49	49	0.001	80	64	0.009
MTi1	233	226	0.007	134	118	0.009
MTi2	193	173	0.012	117	103	0.008

The SEM micrographs (Figure 6) confirmed the changes in the textural properties from the parent montmorillonite to the treated solids, and between both treated solids. Natural montmorillonite had a more spongy aspect, while the deposition of titanium species resulted in a more compact morphology. The surface chemical analyses of the particles showed a good agreement with the bulk chemical analyses obtained by ICP.

These solids were used as catalysts for the photodegradation of 1,2,4-trichlorobenzene (TCB), under the conditions detailed in Section 2.3. Degradation of the compound in the presence of UV light (photolysis), was first investigated. After 50 min of treatment, ca. 85% of the TCB has been degraded, reaching 90% after 150 min. This suggested a strong sensitivity of TCB to UV light, although this result was referred only to disappearance of TCB, and no information was gained on the possible degradation by–products.
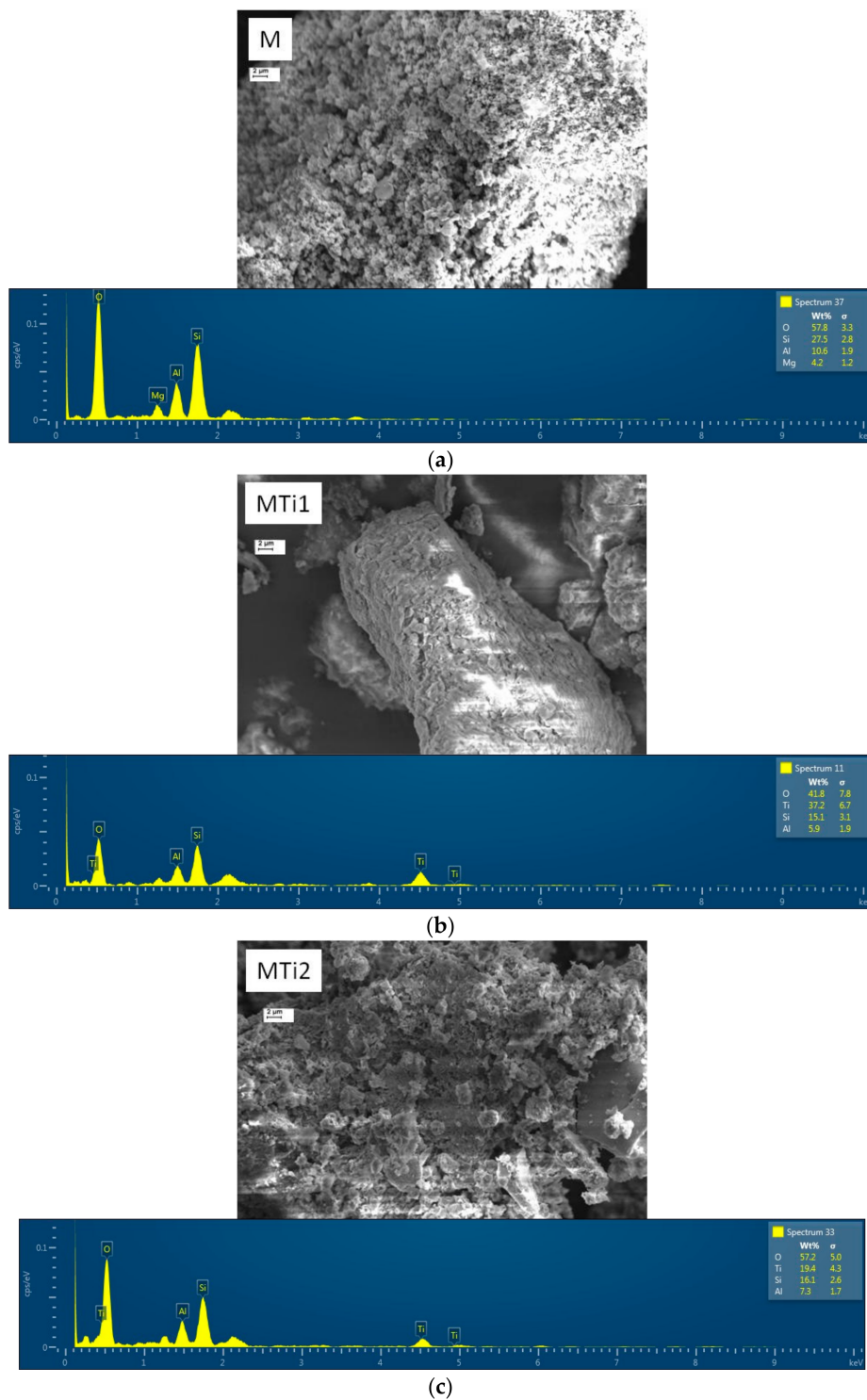
Figure 6. SEM micrographs and point analyses of the parent montmorillonite and the prepared nanocomposites: Montmorillonite (**a**); MTi1 (**b**); and MTi2 (**c**) solids.

To compare the effectiveness of the two nanocomposites and the natural clay, experiments were performed using these samples in the darkness and under UV radiation, as shown in Figure 7. Considering the experiments carried out in the darkness, the natural montmorillonite only removed ~5% of TCB after 240 min. The elimination produced by sample MTi2 was initially zero, and was around 10% after 90 min of reaction, while sample MTi1 immediately produced the elimination of 35%

of the TCB, this value remaining constant over time. Under these conditions, TCB was not expected to be degraded so its elimination may be due to its adsorption on the solids and thus unable to be detected by UV–Vis spectroscopy. The different properties of both nanocomposites, discussed above, should be responsible for their behavior, and as the differences in the textural properties were small, it seemed more likely that their behavior was more influenced by the different nature of the existing titanium species.
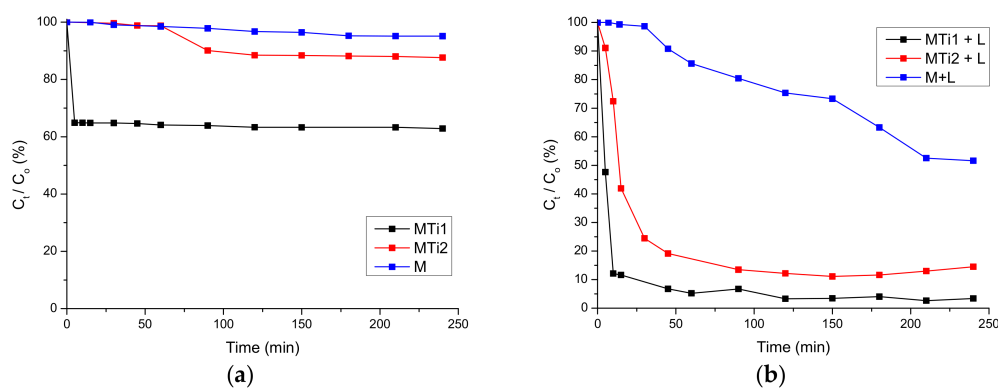
Figure 7. (**a**) Degradation of TCB in darkness and (**b**) under ultraviolet irradiation.

On application of UV radiation, elimination strongly increased with respect to the experiments carried out in the darkness, reaching almost 50% for the natural clay after 210 min. Removal reached 90% after 45 min of reaction for sample MTi1, remaining constant for longer times, while MTi2 sample showed a similar behavior, but reaching a removal of 80%. Photodegradation must be the process responsible for this elimination, especially on comparing both panels in Figure 7. The best behavior of the calcined solids may be related to their capacity for TCB adsorption, clearly evidenced in the experiment carried out in the dark, as once adsorbed, TCB may be more easily degraded on sample MTi1.

Therefore, the nanocomposites showed better performance than parent montmorillonite, proving the importance of the incorporation of Ti, and the catalyst prepared using ultrasounds showed a better performance than that prepared by the traditional method. The catalytic behavior of TiO_2–clay materials catalysts is known to be strongly conditioned by the good dispersion of the TiO_2 particles on the surface of the clay minerals [8,33–35]. Our results confirm this fact, suggesting again that the dispersion obtained by the ultrasonic method was better than that achieved by the traditional method. It is well known that anatase phase is more active than rutile. As shown by the Raman spectroscopy studies reported here, sample MTi1 contained both anatase and rutile phases, while sample MTi2 showed the formation of anatase only, which may suggest that MTi2 should be more active. However, it should be noticed that sample MTi1 fixed a larger amount of TiO_2 than sample MTi2 (Table 2), and thus, even in the presence of rutile, the amount of anatase in sample MTi1 should be larger than in sample MTi2. On the other hand, some studies have demonstrated that anatase-rutile mixtures are beneficial on the charge transfer process during photocatalysis [36,37]. Even more, the presence of amorphous phases in both solids cannot be ruled out, making more difficult any quantitative comparison of the amount of each crystalline phase. In any case, it is clear that the solid prepared under ultrasounds was more active in the photocatalytic reaction.

As commented before, determination of TCB concentration in solution by UV–visible spectroscopy allows to evaluate the removal of this compound, but it does not give any information on the degradation route, the generation of by–products, etc. In order to gain insight in the nature of the by-products formed, the solutions were studied by mass spectrometry after various photodegradation experiments. Representative spectra are shown in Figure 8 (the whole spectra, in larger size plots, are also given in Figure S2). Both catalysts produced a fast degradation of TCB; in fact, the molecular peak only appeared in the solution treated with MTi1 for 5 min, or for 5 and 15 min with MTi2.

The molecular peak appeared between m/z 180 and 183 amu, in agreement with the presence of the different isotopes of chlorine. Longer treatments with any of the catalysts produced the complete disappearance of the molecular peak.

In addition to the molecular peak, all spectra showed peaks with m/z ratios of 145–147, 109–110 and 74–75, readily attributable to the species resulting from the loss of one, two or the three chlorine atoms, respectively, initially existing in the molecule. In the treatments carried out with both catalysts for 5 min, the molecular peak was still the most intense one, while the peaks corresponding to the fragments after chlorine loss showed progressively decreasing intensities. This suggested that chlorine atoms were released consecutively, not simultaneously. In the spectrum of the sample treated with MTi2 for 15 min the intensity of the molecular peak decreased noticeably, indicating the advance of the degradation, and the intensity of the peaks of the by-products showed that under these conditions, the loss of the three chlorine atoms was predominant.

Other significant peaks (50, 59, 265, 293 amu) were also recorded in the spectra, especially after the longer treatments, indicating the presence of numerous fragments of different masses, and suggesting that the benzene ring could be broken at different positions, and the same would happen to the resulting by–products. It was striking that after treatment with MTi1 for 5 min new peaks appeared at m/z 265 and 293 amu, larger than the molecular peak. The second peak can be tentatively assigned to the formula $C_{12}H_7Cl_4^+$, that is, the result of protonating the dimer that would result from the binding of two dichlorobenzene entities. This suggested that after the initial loss of a chlorine atom from the TCB molecule, two fragments reacted to form the dimer, which would subsequently break down and continue its degradation. The peak at m/z 265 amu could correspond to the degradation of the dimer, implying the opening of one of the rings and the elimination of carbon atoms from the resulting chain, or to the binding of the TCB molecule to some of the fragments previously obtained during the degradation. In any case, although these intermediates were formed, they later continued their degradation. However, it may be considered that these intermediates would probably show absorption peaks in the UV region, thus influencing the determination of the removal of TCB by UV spectroscopy.
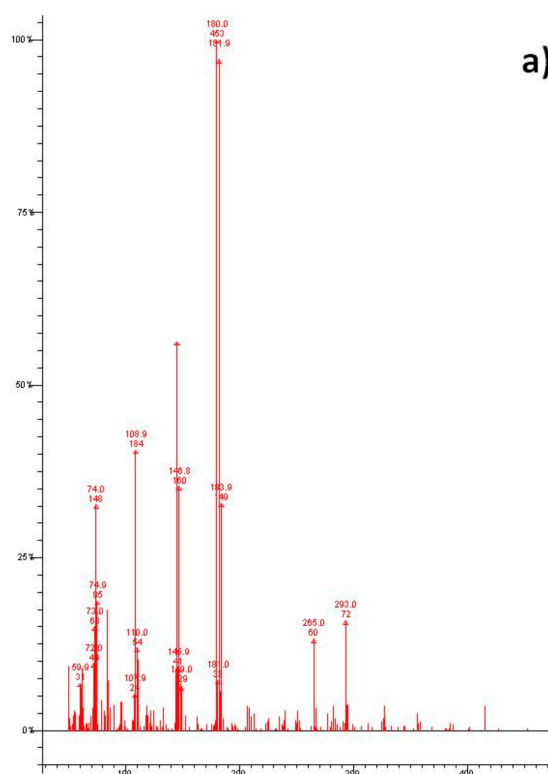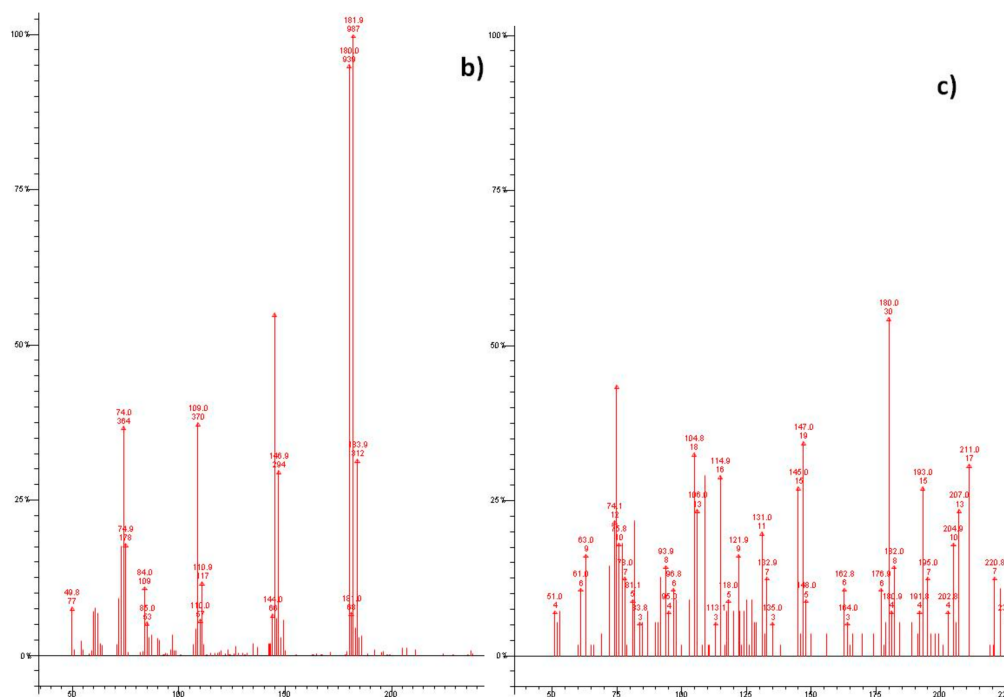

Figure 8. *Cont.*

Figure 8. Mass spectra of the solutions obtained after photocatalytic treatment of TCB using MTi1 catalyst for 5 min (**a**) and MTi2 for 5 (**b**) or 15 (**c**) minutes.

4. Conclusions

Solids based on montmorillonite–TiO_2 nanocomposites have been prepared, with large basal spacing and high specific surface area values. The properties of the nanocomposites were rather different if the preparation method involved simple stirring or ultrasound irradiation. Both solids were active in the photodegradation of 1,2,4-trichlorobenzene, with the nanocomposite prepared under ultrasound irradiation showing a better performance. The degradation of 1,2,4-trichlorobenzene was very fast, and began by the removal of the chlorine atoms, also involving the dimerization of the benzene ring, and the bonding to the ring of fragments previously removed from other molecules.

References

1. Adams, J.M.; McCabe, R.W. Clay Minerals as Catalysts. In *Handbook of Clay Science*; Developments in Clay Science; Bergaya, F., Theng, B.K.G., Lagaly, G., Eds.; Elsevier Ltd.: Amsterdam, The Netherland, 2006; ISBN 9780080457635.
2. Elbokl, T.A.; Detellier, C. Intercalation of cyclic imides in kaolinite. *J. Colloid Interface Sci.* **2008**, *32*, 338–348. [CrossRef] [PubMed]

3.	Gil, A.; Korili, S.A.; Trujillano, R.; Vicente, M.A. (Eds.) *Pillared Clays and Related Catalysts*; Springer: Berlin, Germany, 2010; ISBN 9781441966698.

4.	Vicente, M.A.; Gil, A.; Bergaya, F. Pillared Clays and Clay Minerals. In *Handbook of Clay Science*, 2nd ed.; Bergaya, F., Lagaly, G., Eds.; Elsevier: Amsterdam, The Netherlands, 2013; Chapter 10.5; ISBN 9780080993713.

5.	Deng, F.; Zhao, X.; Pei, X.; Luo, X.; Li, W.; Au, C. Sol–Hydrothermal Synthesis of Inorganic Framework Molecularly Imprinted TiO_2 Nanoparticle and its Enhanced Photocatalytic Activity for Degradation of Target Pollutant. *Sci. Adv. Mater.* **2016**, *8*, 1079–1085. [CrossRef]

6.	Lewis, N.S.; Rosenbluth, M.L. Theory of Semiconductor Materials. In *Photocatalysis: Fundamentals and Applications*; Serpone, N., Pelizzetti, E., Eds.; John Wiley & Sons: Hoboken, NJ, USA, 1989; pp. 45–99. ISBN 978-0471626039.

7.	Kocí, K.; Matejka, V.; Kovár, P.; Lacny, Z.; Obalová, L. Comparison of the pure TiO_2 and kaolinite/TiO_2 composite as catalyst for CO_2 photocatalytic reduction. *Catal. Today* **2011**, *161*, 105–109. [CrossRef]

8.	Mathew, R.; Khan, S.U. Photodegradation of Metolachlor in Water in the Presence of Soil Mineral and Organic Constituents. *J. Agric. Food Chem.* **1996**, *44*, 3996–4000. [CrossRef]

9.	Zhang, Y.; Gan, H.; Zhang, G. A novel mixed–phase TiO_2/kaolinite composites and their photocatalytic activity for degradation of organic contaminants. *Chem. Eng. J.* **2011**, *172*, 936–943. [CrossRef]

10.	Papoulis, D.; Komarneni, S.; Panagiotaras, D.; Stathatos, D.; Christoforidise, K.C.; Fernández–García, M.; Li, H.; Shu, Y.; Sato, T.; Katsuki, H. Three–phase nanocomposites of two nanoclays and TiO_2: Synthesis, characterization and photocatalytic activities. *Appl. Catal. B* **2014**, *147*, 526–533. [CrossRef]

11.	Mamulová Kutláková, K.; Tokarský, J.; Kovář, P.; Vojtěšková, S.; Kovářová, A.; Smetana, B.; Kukutschová, J.; Čapková, P.; Matějka, V. Preparation and characterization of photoactive composite kaolinite/TiO_2. *J. Hazard Mater.* **2011**, *188*, 212–220. [CrossRef] [PubMed]

12.	Ray, S.; Sedev, R.; Priest, C.; Ralston, J. Influence of the Work of Adhesion on the Dynamic Wetting of Chemically Heterogeneous Surfaces. *Langmuir* **2008**, *24*, 13007–13012. [CrossRef] [PubMed]

13.	Zhao, J.C.; Wu, T.X.; Wu, K.Q.; Oikawa, K.; Hidaka, H.; Serpone, N. Photoassisted Degradation of Dye Pollutants. 3. Degradation of the Cationic Dye Rhodamine B in Aqueous Anionic Surfactant/TiO_2 Dispersions under Visible Light Irradiation: Evidence for the Need of Substrate Adsorption on TiO_2 Particles. *Environ. Sci. Technol.* **1998**, *32*, 2394–2400. [CrossRef]

14.	Wang, Q.; Chen, C.C.; Zhao, D.; Ma, W.H.; Zhao, J.C. Change of adsorption modes of dyes on fluorinated TiO_2 and its effects on photocatalytic degradation of dyes under visible irradiation. *Langmuir* **2008**, *24*, 7338–7345. [CrossRef] [PubMed]

15.	Xu, Y.M.; Langford, C.H. Photoactivity of Titanium Dioxide Supported on MCM41, Zeolite X and Zeolite Y. *J. Phys. Chem. B* **1997**, *101*, 3115–3121. [CrossRef]

16.	Peng, T.Y.; Zhao, D.; Dai, K.; Shi, W.; Hirao, K. Synthesis of Titanium Dioxide Nanoparticles with Mesoporous Anatase Wall and High Photocatalytic Activity. *J. Phys. Chem. B* **2005**, *109*, 4947–4952. [CrossRef] [PubMed]

17.	Miao, S.D.; Liu, Z.M.; Han, B.X.; Zhang, J.L.; Yu, X.; Du, J.M.; Sun, Z.Y. Synthesis and characterization of TiO_2–montmorillonite nanocomposites and their application for removal of methylene blue. *J. Mater. Chem.* **2006**, *16*, 579–584. [CrossRef]

18.	Hong, H.L.; Jiang, W.T.; Zhang, X.L.; Tie, L.Y.; Li, Z.H. Adsorption of Cr(VI) on STAC–modified rectorite. *Appl. Clay Sci.* **2008**, *42*, 292–299. [CrossRef]

19.	Li, Z.H.; Jiang, W.T.; Chen, C.J.; Hong, H.L. Influence of Chain Lengths and Loading Levels on Interlayer Configurations of Intercalated Alkylammonium and Their Transitions in Rectorite. *Langmuir* **2010**, *26*, 8289–8294. [CrossRef] [PubMed]

20.	Yang, H.M.; Tang, A.D.; Ouyang, J.; Li, M.; Mann, S. From Natural Attapulgite to Mesoporous Materials: Methodology, Characterization and Structural Evolution. *J. Phys. Chem. B* **2010**, *114*, 2390–2398. [CrossRef] [PubMed]

21.	Khataee, A.; Sheydaei, M.; Hassani, A.; Taseidifar, M.; Karaca, S. Sonocatalytic removal of an organic dye using TiO_2/Montmorillonite nanocomposite. *Ultrason. Sonochem.* **2015**, *22*, 404–411. [CrossRef] [PubMed]

22.	Kun, R.; Mogyorósi, K.; Dékány, I. Synthesis and structural and photocatalytic properties of TiO_2/montmorillonite nanocomposites. *Appl. Clay Sci.* **2006**, *32*, 99–110. [CrossRef]

23.	Zhang, G.K.; Ding, X.M.; He, F.S.; Yu, X.Y.; Zhou, J.; Hu, Y.J.; Xie, J.W. Low-temperature synthesis and photocatalytic activity of TiO_2 pillared montmorillonite. *Langmuir* **2008**, *24*, 1026–1030. [CrossRef] [PubMed]

24. González–Rodríguez, B.; Trujillano, R.; Rives, V.; Vicente, M.A.; Gil, A.; Korili, S.A. Structural, textural and acidic properties of Cu–, Fe– and Cr–doped Ti–pillared montmorillonites. *Appl. Clay Sci.* **2015**, *118*, 124–130. [CrossRef]

25. Rouquerol, F.; Rouquerol, J.; Sing, K. *Adsorption by Powders and Porous Solids—Principles, Methodology and Applications*; Academic Press: Cambridge, MA, USA, 1998; ISBN 978-0-12-598920-6.

26. Vicente, M.A.; Belver, C.; Trujillano, R.; Suárez, M.; Bañares, M.A.; Rives, V. Improvement of the properties of natural clays by acid activation. In *Applied Study of Cultural Heritage and Clays*; Pérez Rodríguez, J.L., Ed.; Biblioteca de Ciencias n° 13; Consejo Superior de Investigaciones Científicas: Madrid, España, 2003; pp. 519–535, ISBN 978-84-00-08197-3.

27. Hanaor, D.A.H.; Sorrell, C.C. Review of the anatase to rutile phase transformation. *J. Mater. Sci.* **2011**, *46*, 855–874. [CrossRef]

28. Ranade, M.R.; Navrotsky, A.; Zhang, H.Z.; Banfield, J.F.; Elder, S.H.; Zaban, A.; Borse, P.H.; Kulkarni, S.K.; Doran, G.S.; Whitfield, H.J. Energetics of nanocrystalline TiO_2. *Proc. Natl. Acad. Sci. USA* **2002**, *99*, 6476–6481. [CrossRef] [PubMed]

29. Porto, S.P.S.; Fleury, P.A.; Damen, T.C. Raman Spectra of TiO_2, MgF_2, ZnF_2, FeF_2, and MnF_2. *Phys. Rev.* **1967**, *154*, 522–526. [CrossRef]

30. Beattie, I.R.; Gilson, T.R. Single crystal laser Raman spectroscopy. *Proc. R. Soc. Lond. A* **1968**, *307*, 407–429. [CrossRef]

31. Vicente, M.A.; Bañares–Muñoz, M.A.; Toranzo, R.; Gandía, L.M.; Gil, A. Influence of the Ti precursor on the properties of Ti–pillared smectites. *Clay Miner.* **2001**, *36*, 125–138. [CrossRef]

32. Sing, K.S.W.; Everett, D.H.; Haul, R.A.W.; Moscou, L.; Pierotti, R.A.; Rouquerol, J.; Siemieniewska, T. Reporting physisorption data for gas/solid systems with special reference to the determination of surface area and porosity. *Pure Appl. Chem.* **1985**, *57*, 603–619. [CrossRef]

33. Barbosa, L.V.; Marçal, L.; Nassar, E.J.; Calefi, P.S.; Vicente, M.A.; Trujillano, R.; Rives, V.; Gil, A.; Korili, S.; Ciuffi, K.J.; et al. Kaolinite–titanium oxide nanocomposites prepared via sol–gel as heterogeneous photocatalysts for dyes degradation. *Catal. Today* **2015**, *246*, 133–142. [CrossRef]

34. Papoulis, D.; Komarneni, S.; Panagiotaras, D.; Stathatos, E.; Toli, D.; Christoforidis, K.C.; Fernandez Garcia, M.; Li, H.; Yin, S.; Sato, T.; et al. Halloysite–TiO_2 nanocomposites: Synthesis, characterization and photocatalytic activity. *Appl. Catal. B* **2013**, *132–133*, 416–422. [CrossRef]

35. Papoulis, D.; Komarneni, S.; Nikolopoulou, A.; Tsolis-Katagas, P.; Panagiotaras, D.; Kacandes, H.G.; Zhang, P.; Yin, S.; Satog, T.; Katsuki, H. Palygorskite–and Halloysite–TiO_2 nanocomposites: Synthesis and photocatalytic activity. *Appl. Clay Sci.* **2010**, *50*, 118–124. [CrossRef]

36. Lei, S.; Duan, W. Highly active mixed-phase TiO_2 photocatalysts fabricated at low temperature and the correlation between phase composition and photocatalytic activity. *J. Environ. Sci.* **2008**, *20*, 1263–1267. [CrossRef]

37. Rives, V. Preparation of titania nanoparticles and relationships between procedures and properties. In *New Developments in Metal Oxides Research*; Nagy, I., Balogh, A., Eds.; Nova Science Publishers: New York, NY, USA, 2013; Chapter 1; ISBN 9781628081480.